

# Zero-delay Consistent and Smooth Trainable Interpolation

Emilio Ruiz-Moreno\*, Luis Miguel López-Ramos\*, and Baltasar Beferull-Lozano\*<sup>†</sup>, *Senior Member, IEEE*

\*WISENET Center, Department of ICT, University of Agder, Grimstad, Norway

<sup>†</sup> SimulaMet, Simula Research Laboratory, Oslo, Norway

**Abstract**—The question of how to produce a smooth interpolating curve from a stream of data points is addressed in this paper. To this end, we formalize the concept of real-time interpolator (RTI): a trainable unit that recovers smooth signals that are consistent with the received input samples in an online manner. Specifically, an RTI works under the requirement of producing a function section immediately after a sample is received (zero delay), without changing the reconstructed signal in past time sections. This work formulates the design of spline-based RTIs as a bi-level optimization problem. Their training consists in minimizing the average curvature of the interpolated signals over a set of example sequences. The latter are representative of the nature of the data sequence to be interpolated, allowing to tailor the RTI to a specific signal source. Our overall design allows for different possible schemes. In this work, we present two approaches, namely, the parametrized RTI and the recurrent neural network (RNN)-based RTI, including their architecture and properties. Experimental results show that the two proposed RTIs can be trained in a data-driven fashion to achieve improved performance (in terms of the curvature loss metric) with respect to a myopic-type RTI that only exploits the local information at each time sample, while maintaining smooth, zero-delay, and consistency requirements.

**Index Terms**—Online optimization, spline interpolation, recurrent neural networks, bi-level optimization.

## I. INTRODUCTION

Time series data are often transferred and stored in reduced or compressed forms. In several practical applications, such as industrial sensor data streams in the oil and gas sector, data reduction schemes are based on non-uniform subsampling, where the samples to be eliminated are determined by the properties of the signal to be compressed. One main advantage of this type of data reduction is that the reconstruction or decompression is done by means of an interpolation procedure.

One common motivation for applying data-reduction is to allow efficient storing of collections of time series for a posterior analysis in batch form. In huge cyber-physical systems, the amount of information collected by pervasive sensors can be overwhelmingly large. In resource-constrained systems that can only retain the most recent data, discarding older data points can hinder the opportunity of learning in batch mode [1], [2]. An alternative to batch processing is online processing using techniques to learn from data in a streaming fashion [3]. Online learning allows extracting information from currently available data before it is discarded and creates the opportunity to analyze streams of data generated at high rates

with the lowest delay possible in order to arrive at actionable intelligence [4].

Consider a practical scenario where several streams of sensor measurements are being collected and sent through a communication channel to a data center where they are consumed by machine learning algorithms that process data in streaming. If the communication channel is limited or expensive, a data reduction scheme must be applied at the sensory side; and a reliable decompression procedure must be executed at the receiver side where the reconstructed data stream is processed. An example of such a practical scenario is the collection of data from sensors in oil and gas platforms and its transmission via satellite links to onshore data centers [5], [6].

In particular, the widespread PI system [7], [8], [9], [10] is a (lossy) data reduction technique that subsamples an input signal in such a way that the original time series can be approximately recovered by means of linear interpolation. Linear interpolation has the advantage of being simple to implement without delay, but the interpolated signals are non-smooth. Many signals in physical systems are smooth, so a compression-decompression system that preserves the smoothness of the input signals is desirable.

Interpolation techniques allow to estimate a continuous signal within the range (set of values of the independent variable between its minimum and maximum) of the sampled data points. Various interpolation methods have been used since ancient times [11], but it was not until more recent times that its mathematical foundations were established [12]. Interpolation can be understood in two slightly different senses: i) *consistent* interpolation where the estimate passes through all the data points; and ii) *smoothing* interpolation where the estimate is enforced to be close to the data points, minimizing a certain fitting metric. In this paper, focus is put in the first type of interpolation.

Some interpolation-based solutions have shown promising results in areas where reliability of a designed system depends on the quality of a function reconstruction under low-delay constraints, such as online reconstruction of biosignals [13] or industrial manipulator trajectories [14], [15]. Among them, spline-based approaches [16], [17] can naturally accommodate smoothness requirements while being applicable in the field of real-time interpolation of streamed time-series data. As an example, the works [18], [19] aim to recover the target signal by joining the centroids of every two consecutive data points. However, this type of procedure is not suitable in the scenario where the streamed data are in the form of intervals (e.g.,

This work was supported by the SFI Offshore Mechatronics grant 237896/O30 and the IKTPLUSS INDURB grant 270730/O70.

quantization intervals). Not exploiting completely the information contained within the sampled data intervals makes it more restrictive and can result into inaccurate signal estimates. In addition, these methods do not let the user choose the order or the degree of smoothness [cf. Sec. II-C] of the spline.

As an alternative approach, penalized regression methods estimate an underlying signal either from noisy samples or uncertainty intervals, by minimizing a weighted combination of a fitness measure and a regularizing term that enforces that the interpolated signal has a certain property such as smoothness.

Kernel-based penalized regression approaches [20], [21], [22] and its online variants [23], allow to estimate complex signals by finding non-linear patterns at a moderate computational cost. Within the framework of streamed time-series, sliding-window-based methods have been proposed to increase the reliability of the reconstruction by processing consecutive data points concurrently. The algorithm proposed in [24] can be easily adapted to interval data points by modifying the functional cost. However, it relies on a matrix inversion or a gradient-based solver if the modified cost does not accept a closed-form solution, making it computationally demanding and unsuitable in low-delay scenarios. On the other hand, some works such as [25], [26] provide low-delay responses by running a single processing iteration over the interval samples in a shifting window every time a sample is received. Unfortunately, they are not able to guarantee that the reconstructed signal passes through all the interval data points (consistent reconstruction), yielding a less reliable function estimate. Another challenge is that online kernel-based approaches propose a signal estimate whose complexity grows linearly with the number of samples. This is a direct consequence of the Representer Theorem [27], and it has two main drawbacks. First, the curse of kernelization [28], i.e., unbounded linear growth in model size and update time with the amount of data, making them dependent on complexity control mechanisms [29], [30]. Second, the additive nature of the function estimate, which may modify the past reconstruction every time a new interval data point is processed, hence affecting the reliability of the function estimate. Consequently, alternative approaches must be sought when, in addition to the smoothness and low-delay requirements, one needs to enforce reliability.

Recent work has explored the use of recurrent neural networks (RNNs) in the context of signal interpolation. In particular, [31] addresses the problem of supervised learning from irregularly sampled multivariate time series by means of a (semi-parametric) interpolation followed by an RNN. In the different but related context of learning under missing data samples, [32] develops several modified versions of the gated recurrent unit (GRU) [33] which account for missing samples in the input data. The aforementioned works combine an interpolation technique with an RNN to perform supervised learning. Differently, our work investigates the use of RNNs for creating the ability to interpolate any two consecutive interval data points with a continuous (potentially up to any degree) polynomial function with low curvature and without knowing the subsequent data points.

More specifically, this paper proposes a zero-delay spline-

based interpolator specifically engineered to be able to reconstruct from non-uniformly sampled signals whose data points are given as non-uniformly sized intervals. An interesting use case is reconstructing non-uniformly sampled and quantized streamed signals.

The main contributions presented in this paper can be summarized as follows:

- We provide the online optimization formulation of a spline-based real-time interpolator (RTI) with zero-delay and which ensures consistency in the reconstruction (reconstructed signal samples pass through a given input sequence of intervals) while minimizing at the same time the curvature. Furthermore, our formulation allows the selection of both the order of the spline and its degree of smoothness.
- The solution to the RTI design problem is expressed as a policy that internally solves a parameterized optimization problem, yielding a bi-level optimization formulation. To the best of our knowledge, our approach is the first one to formulate the online zero-delay interpolation as a bi-level optimization problem.
- The optimality of the solutions of the RTI design problem naturally leads to the design of policies such that, every time a new interval data sample arrives, the RTI updates the signal estimate without affecting the so far reconstructed signal. Due to the nature of the spline, new updates do not require to update the previous reconstruction (as opposed to other popular methods, e.g. kernel methods), substantially decreasing the complexity.
- We design two different RTI architectures, namely, the parametrized RTI, and the RNN-based RTI, including their properties and a procedure to train them from example data sequences. In this way, their performance can be improved with respect to a Myopic RTI that only exploits the local information at each time sample, while maintaining smooth, zero-delay, and consistency requirements. The training procedure allows also to train different RTIs tailored to different signal sources.
- The proposed RTI design methodology is flexible enough to accommodate different alternative approaches (e.g. neural architectures) in addition to the two specific architectures proposed in the paper.
- We present experimental results where we have carried out training, validation and testing, showing the effectiveness of the two proposed RTIs, in terms of the curvature loss metric.

The paper is structured as follows: Sec. II sets the notation and presents some basic concepts and definitions. Then, in Sec. III we formulate the problem addressed in this paper. Next, in Sec. IV and Sec. V we respectively provide and validate a solution. Finally, Sec. VI concludes the paper.

## II. PRELIMINARIES

In this section, we clarify the notation, introduce fundamental definitions and address some basic concepts that appear recurrently along the paper.

### A. Notation

Vectors and matrices are represented by bold lowercase and bold capital letters respectively. Given a vector  $\mathbf{v} = [v_1, \dots, v_D]^\top \in \mathbb{R}^D$ , where  $D \in \mathbb{N}$  denotes its dimensionality, its  $d$ th component is denoted as  $[v]_d \triangleq v_d$ . Similarly, given a matrix  $\mathbf{M} \in \mathbb{R}^{R \times C}$ , the element in the  $r$ th row and  $c$ th column is denoted as  $[\mathbf{M}]_{r,c}$ . Finally, the notation  $[v]_{i:j}$  refers to the *sliced* vector  $[v_i, \dots, v_j]^\top \in \mathbb{R}^{j-i+1}$ .

### B. Basic definitions

In this paper, we deal with streamed data in the form of sequential time-series conformed by quantized data samples, or *intervals*.

An interval  $\iota$  is described by its time stamp  $x \in \mathbb{R}$ , centroid  $y \in \mathbb{R}$  and half interval step size  $\epsilon \in \mathbb{R}_+$ , i.e.,  $\iota = (x, y, \epsilon)$ . A set of intervals ordered in time is denoted here as a *sequence* where the  $n$ th interval is  $\iota_n = (x_n, y_n, \epsilon_n)$ . The interval associated time stamps are set in strictly monotonically increasing order, i.e.  $x_{n-1} < x_n$  for all time stamps in the sequence. Any two consecutive time stamps define a *time section*  $\mathcal{T}_n = (x_{n-1}, x_n]$  with the exception of  $\mathcal{T}_0 = \{x_0\}$ . We denote a sequence of intervals as  $\mathcal{Z} = \{\iota_n\}_{n=1}^N$ , where  $N$  refers to its length.

1) *Curvature*: Consider the space  $\mathcal{F}_{\mathcal{D}}$  of continuous functions  $f$ , with first continuous derivative and second derivative square integrable, over the domain  $\mathcal{D} \subseteq \mathbb{R}$ . Then, we can define the (one-dimensional) curvature ([20], p.5) for any  $f \in \mathcal{F}_{\mathcal{D}}$  as

$$\kappa(f) \triangleq \int_{\mathcal{D}} \left( \frac{d^2}{dt^2} f(t) \right)^2 dt = \int_{\mathcal{D}} \left( f^{(2)}(t) \right)^2 dt. \quad (1)$$

Intuitively it measures how far a function  $f \in \mathcal{F}_{\mathcal{D}}$  is from having a linear behaviour.

2) *Consistency*: The term consistency refers to the property of any reconstructed signal falling into all intervals of a given sequence [34]. Mathematically,  $f$  is consistent with the sequence  $\mathcal{Z}$  if and only if  $|f(x_n) - y_n| \leq \epsilon_n$  for all the elements in the sequence of intervals, i.e.,  $\forall n \in [1, N]$ .

### C. Spline

A spline is a piecewise-defined function where each piece or *function section* is a polynomial. Each function section contributes actively on its respective time section.

Any spline composed by  $n$  function sections can be expressed as

$$f_n(t) = \begin{cases} g_0(t), & \text{if } t = x_0 \\ g_1(t), & \text{if } x_0 < t \leq x_1 \\ \vdots & \\ g_n(t), & \text{if } x_{n-1} < t \leq x_n \end{cases} \quad (2)$$

where every function section  $g_i : \mathcal{T}_i \rightarrow \mathbb{R}$  is a linear combination of polynomials

$$g_i(t) = \mathbf{a}_i^\top \mathbf{p}_i(t) \quad (3)$$

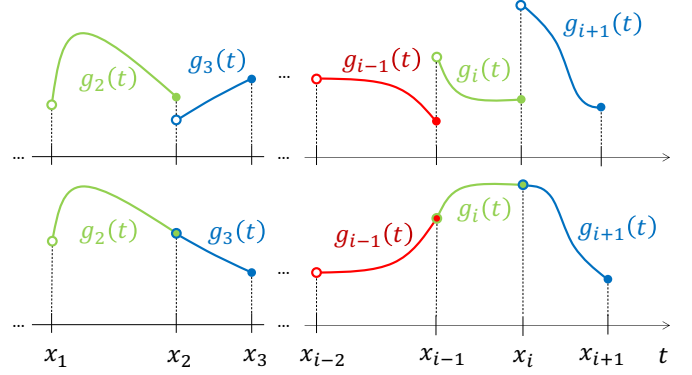


Fig. 1. Non-continuous spline vs. continuous spline.

with combination coefficients  $\mathbf{a}_i \in \mathbb{R}^{d+1}$  and the basis function vector  $\mathbf{p}_i : \mathbb{R} \rightarrow \mathbb{R}^{d+1}$  set as

$$\mathbf{p}_i(t) = [1, (t - x_{i-1}), \dots, (t - x_{i-1})^d]^\top, \quad (4)$$

for all  $t \in \mathcal{T}_i$ . The parameter  $d$  denotes the *order* of the spline and it is user-defined in practice.

We say that a spline  $f_n$  has a degree of *smoothness*  $m$ , or equivalently that is of class  $C^m$ , if it has  $m$  continuous derivatives over the interior of its domain  $\text{dom}(f_n) = \bigcup_{i=0}^n \mathcal{T}_i$ . In order to compute the curvature of a spline  $f_n$ , as in (1), it must belong to the space  $\mathcal{F}_{\bigcup_{i=0}^n \mathcal{T}_i}$ . Every spline  $f_n$  is composed by  $n$  function sections and  $n-1$  *contact* points. We say that two consecutive function sections have a contact of order  $m$ , at the union point, if they have  $m$  equal derivatives. Clearly every  $i$ th function section  $g_i$ , defined over its time section  $\mathcal{T}_i$ , belongs to  $\mathcal{F}_{\mathcal{T}_i}$ . Hence, for  $f_n$  to belong to  $\mathcal{F}_{\bigcup_{i=0}^n \mathcal{T}_i}$  we additionally need to ensure that the contact points are at least of order  $m \geq 1$ , see Fig. 1.

In practice this can be enforced by imposing, at the contact points, the following equality constraint of continuity:

$$\lim_{t \rightarrow x_{i-1}^-} g_{i-1}^{(k)}(t) = \lim_{t \rightarrow x_{i-1}^+} g_i^{(k)}(t), \quad (5)$$

for every  $k \in \mathbb{N}^{[0,m]}$  and  $i \in \mathbb{N}^{[1,n]}$ , where the super index  $(k)$  denotes the  $k$ th derivative with respect to time.

**Result 1.** The constraint in (5) can be rewritten as

$$[\mathbf{a}_i]_{1:m+1} = \mathbf{e}_i, \quad (6)$$

for every  $i \in [1, n]$  where  $\mathbf{a}_i$  contains the combination coefficients of the  $i$ th function section and  $\mathbf{e}_i \in \mathbb{R}^{m+1}$  is a vector such that each of its elements is defined as

$$[\mathbf{e}_i]_q = \frac{1}{(q-1)!} \sum_{j=1}^{d+1} [\mathbf{a}_{i-1}]_j h_{i-1}^{j-q} \prod_{\ell=1}^{q-1} (j-\ell), \quad (7)$$

where  $h_{i-1} \triangleq x_{i-1} - x_{i-2}$ , with the exception of  $h_0 = 0$ .

See Appendix B for the derivation.

### III. PROBLEM FORMULATION

With the definitions provided in Sec. II, we are ready to discuss the different ways to formulate the interpolation problem.

### A. Batch interpolation

Given the whole sequence of intervals  $\mathcal{Z}$ , the function that consistently reconstructs the original signal with minimum curvature, is the solution to the (batch) interpolation problem, formulated as

$$\begin{aligned} & \underset{f \in \mathcal{F}_{[x_1, x_N]}}{\text{minimize}} \quad \kappa(f) \\ & \text{subject to:} \quad |f(x_i) - y_i| \leq \epsilon_i, \forall i \in [1, N], \end{aligned} \quad (8)$$

whose solution is known as the *natural cubic spline* [35]. The term cubic refers to a spline of order  $d = 3$  with a degree of smoothness  $m = 2$ , and it is termed natural because its second derivative equals zero at the contour points.

In order to solve an interpolation problem in batch form, all intervals must be available. However, in cases where interval data become available sequentially, a different approach is necessary. Moreover, a key observation is that the concept of an optimal solution is not clear anymore and the result of  $d = 3$  and  $m = 2$  being optimal is not necessarily true straightaway.

The sequential case, implying working under the requirement that a function section is reconstructed right after each sample interval is received, is addressed in the ensuing section.

### B. Online zero-delay interpolation

Consider the sequential setting in which the data samples of the sequence  $\mathcal{Z}$  become available one by one.

The goal is to create a *real-time interpolator* (RTI) that, once it receives the  $n$ th data sample, is required to reconstruct the signal segment within the new time section  $\mathcal{T}_n$  without affecting the previous reconstructed function sections. In addition, the resulting reconstructed signal  $f_n$  must be consistent with the sequence of intervals, and it must belong to  $\mathcal{F}_{\bigcup_{i=0}^n \mathcal{T}_i}$ .

Recall that the batch problem (8) is a deterministic optimization problem and comes with a clear sense of optimality associated. When designing an RTI that has to act without knowledge of the ensuing data points, it will become necessary to interpret the interval sequence as a random process<sup>1</sup>. Lastly, among all possible consistent reconstructed function candidates, the RTI must choose the one that reduces the expected curvature (over all possible sequences).

In this work, the focus is put on designing a spline-based RTI, more specifically, using a user-defined spline class of order  $d \in \mathbb{N}$  and degree of smoothness  $m \in \mathbb{N}$  such that  $1 \leq m < d$ . Note that if  $m = d$ , the RTI becomes trivial. The reconstructed signal is built by adjoining function sections that satisfy the aforementioned constraints. When the algorithm proposes a function section, as in (3), it is underlyingly selecting the combination coefficients. Formally, the set of all these possible choices or *actions* is called *action space* and it is denoted as  $\mathcal{A}$ . As soon as a vector of combination coefficients is chosen, the function section is determined because the basis vector is given.

Due to the continuity constraint in (5), an action taken after receiving a certain data point will have an impact on

<sup>1</sup>Characterizing the distribution of the interval sequence as a random process is an interesting approach. However, in this paper, we will adopt a data-driven approach where only sample sequences are utilized.

the function sections reconstructed in the future, hence on the overall curvature. This fact motivates for modeling the real-time interpolation problem in the context of sequential decision making over a state space.

Here, the state space is composed by two subspaces: a) the *input* (the last received interval), and b) the *internal state* in which the interpolation task was left at the previous iteration. In turn, the  $n$ th internal state is composed by the  $n$ th *signal state*,  $c_n$  and the  $n$ th *latent state*,  $\ell_n$ . The signal state  $c_n$  encodes the necessary information to ensure the  $m$  degree of smoothness. The latent state  $\ell_n$  keeps track of a (fixed size) *feature* representation of the sequence. The signal state is uniquely determined after taking an action whereas the latent state depends on how the latent feature space is modeled. Using a latent state space is optional and will be discussed in depth in Sec. IV when the RNN-based policies are introduced. We denote the state space as  $\mathcal{S}$ .

Actions will depend on the current state; therefore, designing an RTI is essentially designing a *policy*, i.e., a function defining how an RTI acts from a specific state. In this work, we focus on *deterministic* policies for simplicity. Formally, a policy can be described by a map  $\pi : \mathcal{S} \rightarrow \mathcal{A}$ . The set of all candidate policies is denoted as  $\Pi$ .

### C. Concept of optimal policy

Among all candidate policies  $\pi \in \Pi$ , the goal is to select the one that minimizes the curvature of the reconstructed signal. While in the batch case, the curvature minimization is a well-defined convex problem, in the sequential case, we have to rely on the expected curvature instead. The optimal policy, denoted by  $\pi^*$ , is defined mathematically as

$$\pi^* \triangleq \arg \min_{\pi \in \Pi} \mathbb{E}_{\mathcal{Z} \sim P_{\mathcal{Z}}} [\kappa(f_{|\mathcal{Z}|})], \quad (9)$$

where  $P_{\mathcal{Z}}$  denotes the probability distribution of sequences and  $|\mathcal{Z}|$  refers to the cardinality or length of the sequence  $\mathcal{Z}$ .

**Theorem 1 (Additivity).** The curvature of a spline  $f_{|\mathcal{Z}|}$  described as in (2), can be computed additively as

$$\kappa(f_{|\mathcal{Z}|}) = \sum_{i=1}^{|\mathcal{Z}|} \kappa(g_i). \quad (10)$$

*Proof:* see Appendix C.

**Theorem 2 (Section curvature).** Given a function section as defined in (3), its curvature can be computed as

$$\kappa(g_i) = \mathbf{a}_i^\top \mathbf{M}_i \mathbf{a}_i, \quad (11)$$

with  $\mathbf{M}_i \in \mathbf{S}_+^{d+1}$  and

$$[\mathbf{M}_i]_{j,k} = \begin{cases} 0 & \text{if } j \leq 2 \text{ or } k \leq 2 \\ \frac{(j-1)(j-2)(k-1)(k-2)}{j+k-5} h_i^{j+k-5} & \text{otherwise,} \end{cases} \quad (12)$$

where  $h_i \triangleq x_i - x_{i-1}$ .

*Proof:* see Appendix D.

As a corollary of theorems 1 and 2 we can equivalently formulate the optimal policy (9) as

$$\pi^* = \arg \min_{\pi \in \Pi} \mathbb{E}_{\mathcal{Z} \sim P_{\mathcal{Z}}} \left[ \sum_{i=1}^{|\mathcal{Z}|} \mathbf{a}_i^\top \mathbf{M}_i \mathbf{a}_i \right] \quad (13)$$

#### D. Empirical optimization of the RTI

In general, the probability distribution  $P_{\mathcal{Z}}$ , introduced in (9), is unknown, thus computing any expectation with respect to it is not possible in practice. Therefore, in this work, we resort to the sample average approximation (estimating the expectation *empirically* as the average over a given set of training data). The aforementioned set of training data is constituted by  $J$  sequences as  $\{\mathcal{Z}^{(j)}\}_{j=1}^J$ .

Hence, instead of solving (13), we aim at solving the following data-driven surrogate optimization problem:

$$\tilde{\pi} \triangleq \arg \min_{\pi \in \Pi} \sum_{j=1}^J \sum_{i=1}^{|\mathcal{Z}^{(j)}|} \mathbf{a}_i^{(j)\top} \mathbf{M}_i^{(j)} \mathbf{a}_i^{(j)}. \quad (14)$$

#### IV. PROPOSED SOLUTION

In this section, we discuss how to design, evaluate and train an RTI as well as its architecture.

##### A. Policy design

Given a spline order  $d$  and degree of smoothness  $m$ , suppose that at time  $n$  we have access to the  $n$ th state  $s_n = (\iota_n, c_n, \ell_n)$ , where the signal state is  $c_n = (x_{n-2}, x_{n-1}, \mathbf{a}_{n-1})$ ,  $x_{-1} = x_0$ , and the latent state  $\ell_n \in \mathbb{R}^L$ .

Then, any policy in the set of feasible policies  $\Pi$  can be written as the result of solving a parameterized convex optimization problem [36], [37], of the form:

$$\mathbf{a}_n = \pi(s_n; \boldsymbol{\theta}) \triangleq \arg \min_{\boldsymbol{\beta} \in \mathbb{R}^{d+1}} \text{cost}_n(\boldsymbol{\beta}, s_n; \boldsymbol{\theta}) \quad (15a)$$

$$\text{subject to: } |\boldsymbol{\beta}^\top \mathbf{p}_n(x_n) - y_n| \leq \epsilon_n, \quad (15b)$$

$$|\boldsymbol{\beta}|_{1:m+1} = \mathbf{e}_n, \quad (15c)$$

where  $\boldsymbol{\theta} \in \mathbb{R}^p$  is a vector containing  $p \in \mathbb{N}$  trainable parameters and the elements of  $\mathbf{e}_n \in \mathbb{R}^{m+1}$  are computed from (7). The reason why we restrict ourselves to policies of the form (15) is because the way they are formulated guarantees the consistency (15b) and smoothness (15c) constraints, and different kinds of policies can be designed by modifying the cost function (15a) without loss of generality.

In this work we describe 3 types of policies, which are not the only possible options since the form of the cost in (15) determines the type of policy.

1) *Myopic policy*: The myopic policy chooses the feasible action that minimizes the *instantaneous* curvature, that is

$$\text{cost}_n(\boldsymbol{\beta}, s_n) = \boldsymbol{\beta}^\top \mathbf{M}_n \boldsymbol{\beta}, \quad (16)$$

with  $\mathbf{M}_n$  given as in (12). Notice that the cost in (16) is invariant with respect to the trainable parameters contained in  $\boldsymbol{\theta}$  and for clarity, we omit its dependency. The myopic policy is not expected to produce the best results but will be used in the experimental Sec. V as a benchmark. Any other proposed policy must outperform the myopic policy to be deemed acceptable.

The myopic policy can be seen as a one-step lookahead policy whose cost-to-go has been set to zero. Notice that knowledge of the exact expected cost-to-go would enable enacting an optimal policy. However, complete knowledge

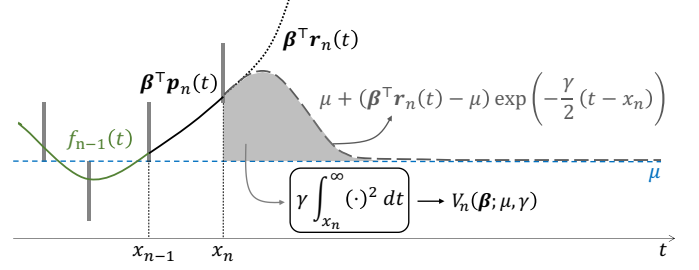


Fig. 2. Visualization of the cost-to-go interpretation for the parametrized policy.

of the distribution of interval sequences would be needed. We can still formulate policies relying on the *parametric* cost-to-go approximation [38], which is typically obtained by using prominent characteristics, or features, of the state. Such features can be designed either through insight into the problem at hand or in a data-driven fashion.

2) *Parametrized policy*: The parametrized policy chooses the feasible action that minimizes a weighted sum between the instantaneous curvature and a parametric cost-to-go representing deviation of future values from typical input intervals of the interpolation signal. Explicitly, the cost consists in

$$\text{cost}_n(\boldsymbol{\beta}, s_n; \boldsymbol{\theta}) = \boldsymbol{\beta}^\top \mathbf{M}_n \boldsymbol{\beta} + \lambda V_n(\boldsymbol{\beta}, s_n; \mu, \gamma), \quad (17)$$

with  $\boldsymbol{\theta} = [\mu, \gamma, \lambda]^\top \in \mathbb{R} \times \mathbb{R}_+^2$  and

$$V_n(\boldsymbol{\beta}, s_n; \mu, \gamma) = \gamma \int_{x_n}^{\infty} (\boldsymbol{\beta}^\top \mathbf{r}_n(t) - \mu)^2 \exp(-\gamma(t - x_n)) dt, \quad (18)$$

where the vector-valued function  $\mathbf{r}_n : \mathbb{R} \rightarrow \mathbb{R}^{d+1}$  is the *analytic continuation*<sup>2</sup> function, of the basis vector (4), over the whole real line.

The main goal of the cost-to-go (18) is to interpolate the signal in such a way that the spline remainder  $\boldsymbol{\beta}^\top \mathbf{r}_n(t)$  is close to the interval samples that are about to come. For this purpose, we assume that the underlying process (generating the sequence  $\mathcal{Z}$ ) is stationary where the parameter  $\mu$  is the time-invariant mean of the process. Moreover, as time instants lying further into the future are harder to predict, we penalize the distance between the  $n$ th remainder and the mean of the process, i.e.,  $\boldsymbol{\beta}^\top \mathbf{r}_n(t) - \mu$ , in the immediate future by weighting it with an exponential window with decay rate  $\gamma$  (which in addition provides certain advantages from the analytical point of view). Intuitively, splines whose remainders deviate more are more likely to incur higher overall curvature. This is because such deviation provokes disadvantageous starting conditions for the next function section. In order to obtain a bounded (finite) and positive metric of such a deviation, the distances are squared and integrated; see Fig. (2) for a visual representation.

**Result 2.** The cost-to-go of the parametrized policy, stated in (18), can be equivalently expressed as

$$V_n(\boldsymbol{\beta}, s_n; \mu, \gamma) = \boldsymbol{\beta}^\top \mathbf{R}_n \boldsymbol{\beta} + \boldsymbol{\beta}^\top \mathbf{v}_n + \mu^2 \quad (19)$$

<sup>2</sup>A technique to extend the domain of definition of a given analytic function.

TABLE I  
 $B_1 = [I_{m+1}, \mathbf{0}_{(m+1) \times (d-m)}]^\top$ ,  $B_2 = [\mathbf{0}_{(d-m) \times (m+1)}, I_{d-m}]^\top$

Myopic	
$D_n$	$B_2^\top M_n B_2$
$\mathbf{o}_n$	$-D_n^{-1} B_2^\top M_n B_1 \mathbf{e}_n$
Parametrized	
$D_n$	$B_2^\top (M_n + \lambda R_n) B_2$
$\mathbf{o}_n$	$-D_n^{-1} (B_2^\top (M_n + \lambda R_n) B_1 \mathbf{e}_n + \frac{1}{2} \lambda B_2^\top \mathbf{v}_n)$
RNN-based	
$D_n$	$B_2^\top (M_n + \lambda I_{d+1}) B_2$
$\mathbf{o}_n$	$-D_n^{-1} (B_2^\top (M_n + \lambda I_{d+1}) B_1 \mathbf{e}_n + \frac{1}{2} \lambda f_\theta(s_n))$

with

$$[\mathbf{R}_n]_{j,k} = \frac{(j+k-2)!}{\gamma^{j+k-2}} \sum_{i=0}^{j+k-2} \frac{(\gamma h_n)^i}{i!}, \quad (20)$$

and

$$[\mathbf{v}_n]_j = -2\mu \frac{(j-1)!}{\gamma^{j-1}} \sum_{i=0}^{j-1} \frac{(\gamma h_n)^i}{i!}. \quad (21)$$

See appendix E for the derivation.

From Result 2 and removing the terms that do not depend on the optimization variable of (15), we can equivalently rewrite the cost in (17) as

$$\text{cost}_n(\boldsymbol{\beta}, s_n; \lambda, \mu, \gamma) = \boldsymbol{\beta}^\top (M_n + \lambda R_n) \boldsymbol{\beta} + \lambda \boldsymbol{\beta}^\top \mathbf{v}_n. \quad (22)$$

**Remark 1.** The cost in (17) is convex with respect to  $\boldsymbol{\beta}$ . See appendix F for a proof.

3) *RNN-based policy*: The recurrent neural network (RNN)-based policy chooses the feasible action that minimizes a weighted sum between the instantaneous curvature and a parametric cost-to-go that penalizes the distance to the output of a certain RNN. Expressly,

$$\text{cost}_n(\boldsymbol{\beta}, s_n; \boldsymbol{\theta}) = \boldsymbol{\beta}^\top M_n \boldsymbol{\beta} + \lambda \left\| \boldsymbol{\beta} - \begin{bmatrix} \mathbf{0}_{m+1} \\ f_\theta(s_n) \end{bmatrix} \right\|_2^2, \quad (23)$$

where  $f_\theta(s_n)$  is the output of an RNN  $f_\theta : \mathcal{S} \rightarrow \mathbb{R}^{d-m}$  evaluated at the state  $s_n$ .

Notice that an RNN that successfully captures the temporal dynamics of the problem, will pull towards the actions that minimize the overall curvature.

## B. Policy evaluation

Evaluating the candidate policies (IV-A1, IV-A2, IV-A3) consists in solving their related optimization problem, as in (15).

**Result 3.** All three candidate policies admit a closed-form evaluation of the form

$$\mathbf{a}_n = \begin{bmatrix} \mathbf{e}_n \\ \boldsymbol{\alpha}_n \end{bmatrix}, \quad (24)$$

where  $\boldsymbol{\alpha}_n \in \mathbb{R}^{d-m}$  is computed as follows

$$\boldsymbol{\alpha}_n = \arg \min_{\boldsymbol{\alpha} \in \mathbb{R}^{d-m}} \|\boldsymbol{\alpha} - \mathbf{o}_n\|_{D_n}^2 \quad (25a)$$

$$\text{subject to: } |\boldsymbol{\alpha}^\top \mathbf{q}_n - z_n| \leq \epsilon_n, \quad (25b)$$

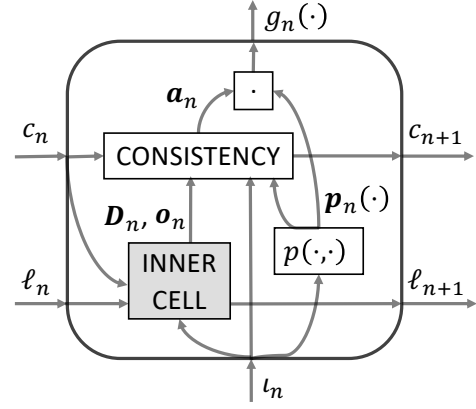


Fig. 3. Visualization of the internal representation of an RTI.

with  $z_n = y_n - \mathbf{e}_n^\top [\mathbf{p}_n(x_n)]_{1:m+1}$ ,  $\mathbf{q}_n = [\mathbf{p}_n(x_n)]_{m+2:d+1}$  and  $D_n$  and  $\mathbf{o}_n$  as in Table I. The optimization problem stated in (25) is commonly referred to as a *hyper slab* projection and admits a closed-form solution. For more details we refer to the Appendix G.

## C. Architecture of the policy

As discussed in Sec. III-B, designing an RTI is essentially designing a policy. At every time step  $n$ , the RTI proposes a function section depending on the status of the state. How such a status is updated depends on the environment and the previous action. Explicitly, the input interval  $\iota_n$  depends completely on the environment, whereas the signal state  $c_n$  and the latent state  $\ell_n$  (if present) depend on both the environment and the previous action  $\mathbf{a}_{n-1}$ .

In this way, the dependencies between the RTI components, resemble a *recurrent cell* or unit [39], (see Fig. 3). All the trainable parameters, and the architecture that relates them, can be encapsulated in an inner cell while the continuity and consistency constraints are imposed through what we call a *consistency layer*. In fact, the consistency layer takes care of solving the convex optimization problem in (15), which is equivalent to evaluating a feasible action. In addition, the output of the consistency layer, which are the spline coefficients, can be differentiated with respect to the trainable parameters, categorizing this layer as a *differentiable convex optimization layer* (DCOL) [36].

From this architecture point of view, the difference between the aforementioned proposed policies lies in the internal structure of the inner cell, while the DCOL is common to all of them. In the case of the myopic policy, the inner cell neither contains any trainable parameter nor uses a latent state. As for the parametrized policy, the inner cell contains three parameters whose interactions have a high degree of associated interpretability. It does not make use of a latent state either. Regarding the RNN-based policy, the inner cell consists in a recurrent unit, such as the well-established GRU or Long Short-term Memory (LSTM) unit [40], among others, which make use of a latent state.

Finally, notice that the scheme in Fig. 3 emphasizes the generalizability of the proposed approach. It can be noticed

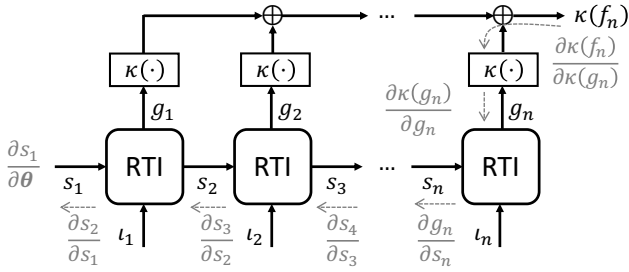


Fig. 4. Schematization of the unrolled RTI.

that alternative RTIs can be built depending on the problem at hand by simply modifying the DCOL and/or the inner cell.

#### D. Policy training

When we consider the training of any of the policies, we refer to optimizing the non-convex optimization problem stated in (14). Recall that the constraint  $\pi \in \Pi$  restricts the candidate policies to the ones of the form given in (15). Therefore, we can explicitly express it within the following *bi-level* [41] optimization problem:

$$\theta^* = \arg \min_{\theta \in \mathbb{R}^p} \sum_{j=1}^J \sum_{i=1}^{|\mathcal{Z}^{(j)}|} \mathbf{a}_i^{(j)\top} \mathbf{M}_i^{(j)} \mathbf{a}_i^{(j)} \quad (26a)$$

$$\text{s. to: } \mathbf{a}_i^{(j)} = \arg \min_{\beta \in \mathbb{R}^{d+1}} \text{cost}_i^{(j)}(\beta, s_n; \theta) \quad (26b)$$

$$\text{s. to: } |\beta^\top \mathbf{p}_i(x_i^{(j)}) - y_i^{(j)}| \leq \epsilon_i^{(j)} \quad (26c)$$

$$[\beta]_{1:m+1} = \mathbf{e}_i^{(j)}. \quad (26d)$$

As mentioned in Sec. IV-C, an RTI can be seen in general as a recurrent unit. Hence, reconstructing a sequence of interval data can be understood as an unfolded RNN and therefore, its parameters can be trained by means of back propagation through time (BPTT) [42], [43], see Fig. 4.

## V. EXPERIMENTAL RESULTS

In this section, we experimentally validate the effectiveness of the proposed trainable RTIs.

For this purpose, we have generated 175 sequences of which 100 have been used for training, 50 for validating and 25 for testing. Each sequence has been originally constructed as a realization of a given autoregressive process AR(1) and each realization is composed of 100 samples. Specifically, for every  $j$ th sequence, each  $n$ th sample has been computed recurrently via  $z_n^{(j)} = \varphi z_{n-1}^{(j)} + u_n^{(j)}$ , with  $z_0^{(j)} = z_1^{(j)}$ , parameter  $\varphi = 0.9$  and Gaussian innovation  $u_n^{(j)} \sim \mathcal{N}(0, 1)$ . Then, we uniformly quantize the samples in every sequence. The centers of the resulting quantization intervals are computed by means of  $y_n^{(j)} = \text{round}(z_n^{(j)}/\epsilon_n^{(j)})$  with a quantization half-step  $\epsilon_n^{(j)} = 0.5$  for all  $j, n$ . The time stamps of every  $j$ th sequence  $\{x_n^{(j)}\}_{n=0}^{100}$  are first uniformly arranged. Then, every sequence is compressed with PI [7], with ExDev = 0.5, ExMax =  $\infty$  and ExMin = 0. As a result, every  $j$ th sequence is not necessarily uniformly sampled anymore (see Fig. 6).

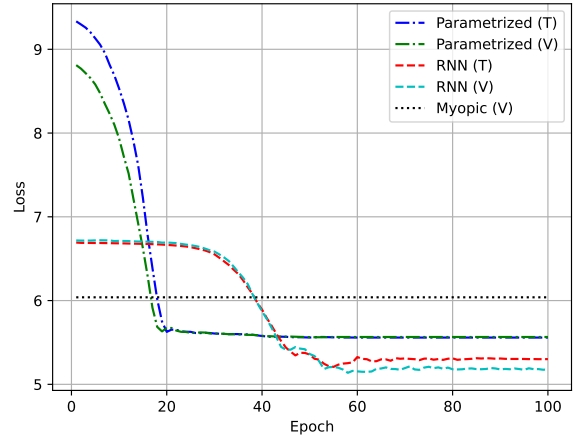


Fig. 5. Training and validation curves. The spline model is of order  $d = 3$  and degree of smoothness  $m = 1$  for all of them. The loss is the average curvature per function section.

TABLE II

	Myopic	Parametrized	RNN-based	Batch
Loss	5.88	5.47	<b>5.22</b>	0.86

Among all possible spline configurations, for the sake of simplicity, we restrict to order  $d = 3$  and degree of smoothness  $m = 1$ . For this experiment, the architecture of the inner cell in the RNN-based policy consists of a GRU cell with 2 layers and a latent state with a feature size of 64.

The validation and training (when applicable) of the myopic RTI and the proposed trainable RTIs are shown in Fig. 5. We have trained the latter using the resilient backpropagation (RPROP) algorithm with full batch, motivated by the fast and accurate results for RNN reported in [44]. As expected, the myopic policy performs better than the random initializations of the trainable RTIs, but it is outperformed by the parametrized and the RNN-based policies once they are trained. As expected, the RNN-policy achieves the best performance. However, its convergence is significantly slower. This behavior is also expected, especially considering the reduced capacity of the parametrized policy in comparison with the RNN-based<sup>3</sup> policy.

To visualize the performance of all the trained RTIs, Fig. (6) shows a snapshot of one of the testing sequences.

To quantify the performance of an RTI, we use the batch solution as a baseline, such that an RTI achieving the same average curvature as the batch solution, would be reported as an improvement of 100% with respect to the myopic policy. The performance over the testing set, see Table II, shows that the parametrized policy improves with respect to the myopic a 8.2% whereas the RNN-based reaches a 13.1% improvement.

<sup>3</sup>Noticeably, the training of the RNN took shorter wallclock time than that of the parametrized policy, despite the higher complexity of the RNN. This is probably because the RNN was implemented using optimized code from the PyTorch library.

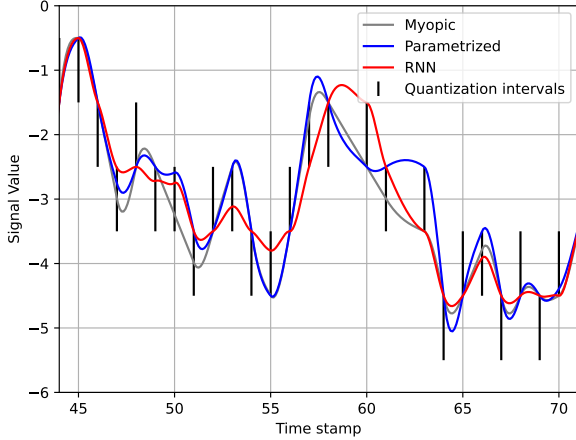


Fig. 6. Example of reconstruction with trained policies.

## VI. CONCLUSION

This paper has formalized the concept of RTI as a trainable unit capable of producing a spline of the desired order and degree of smoothness in an online fashion while receiving a stream of data points or intervals. The proposed RTIs deal with sequences composed of nonuniform quantization intervals and nonuniform sampling time stamps. Such units allow to consistently interpolate a sequence with zero delay, meaning that a function segment covering up to the latest received time stamp is produced immediately after the latest interval has been received.

Defining a myopic (greedy) RTI is relatively straightforward once the question of how to guarantee consistency of the output sequence with the stream of input intervals is addressed [cf. constraints in (15)]. The definition of RTI architectures with the ability to produce an interpolated function with a reduced curvature requires the formulation of alternative objective functions that account for the long-term effects of the choice of a given function section. The sequence of intervals to be interpolated is understood as a random process and the goal is to minimize the expected curvature of the spline produced by the RTI. In practice, a statistical characterization of the interval sequences of a given data source will not be available, so an empirical (data-driven) approach is preferred and has been applied throughout the paper, including the section of experimental results.

The experimental results that have been carried out show that both proposed architectures, namely the RNN-based and the parametrized RTI outperform the myopic policy. Moreover, the RNN-based RTI achieves a better performance and its training time is faster. This promising result motivates further experiments with different network sizes and depths and also using them in experiments with example sequences from real data sources.

## AUTHOR STATEMENT AND ACKNOWLEDGEMENTS

We describe contributions to the paper using the taxonomy provided in [45]. *Conceptualization*: E.R. and L.L.;

*Methodology*: E.R. and L.L.; *Software*: E.R.; *Validation*: E.R.; *Formal analysis*: E.R.; *Investigation*: E.R.; *Writing – Original draft*: E.R. and L.L.; *Writing – Review and Editing*: L.L. and B.B.; *Visualization*: E.R.; *Supervision*: L.L. and B.B.; *Project administration*: B.B.; *Funding acquisition*: B.B.

The authors thank Filippo Sanfilippo for the discussion about potential extension and/or impact of the present work.

## APPENDIX

**Proposition 1 (Positive (semi)-definiteness).** Given a vector-valued real function  $\mathbf{v} : \mathcal{D} \rightarrow \mathbb{R}^d$  with  $\mathcal{D} \subseteq \mathbb{R}$ , the matrix  $\mathbf{W} \in \mathbb{R}^{d \times d}$  constructed as

$$[\mathbf{W}]_{i,j} = \int_{\mathcal{D}} [\mathbf{v}(t)]_i [\mathbf{v}(t)]_j dt, \quad (27)$$

is positive semi-definite. If in addition, the components of  $\mathbf{v}(t)$  are linearly independent, then the matrix  $\mathbf{W}$  is positive definite.

### A. Proof of Proposition 1

To prove positive semi-definiteness of  $\mathbf{W}$ , it suffices to prove that  $\mathbf{z}^\top \mathbf{W} \mathbf{z} \geq 0$  for all  $\mathbf{z} \in \mathbb{R}^d$ . To this end, note that

$$\mathbf{z}^\top \mathbf{W} \mathbf{z} = \int_{\mathcal{D}} \mathbf{z}^\top \mathbf{v}(t) \mathbf{v}(t)^\top \mathbf{z} dt \quad (28a)$$

$$= \int_{\mathcal{D}} (\mathbf{z}^\top \mathbf{v}(t))^2 dt \geq 0. \quad (28b)$$

By definition, if the components of  $\mathbf{v}(t)$  are linearly independent, there is no  $\mathbf{z} \neq \mathbf{0}$  such that  $\mathbf{z}^\top \mathbf{v}(t) = 0$  for  $t \in \mathcal{D}$ . Therefore, if this is the case, the inequality in (28b) is strict, meaning that  $\mathbf{W}$  is positive definite.

### B. Derivation of Result 1

Recall, from (3), that the  $k$ th derivative of the  $i$ th function section can be computed as

$$g_i^{(k)}(t) = \mathbf{a}_i^\top \mathbf{p}_i^{(k)}(t) \quad (29)$$

and from (4), that the  $j$ th component of the  $i$ th basis vector equals

$$[\mathbf{p}_i(t)]_j = (t - x_{i-1})^{j-1} \quad (30)$$

for all  $j \in [1, d+1]$ . Therefore,

$$[\mathbf{p}_i^{(k)}(t)]_j = (t - x_{i-1})^{j-1-k} \prod_{\ell=1}^k (j - \ell), \quad (31)$$

for every  $k \in [0, m]$ .

Now notice that,

$$\lim_{t \rightarrow x_{i-1}^+} [\mathbf{p}_i^{(k)}(t)]_j = \begin{cases} k! & \text{if } j = k+1 \\ 0 & \text{otherwise.} \end{cases} \quad (32)$$

Hence,

$$\lim_{t \rightarrow x_{i-1}^+} g_i^{(k)}(t) = \sum_{j=0}^m [\mathbf{a}_i]_j \lim_{t \rightarrow x_{i-1}^+} [\mathbf{p}_i^{(k)}(t)]_j \quad (33a)$$

$$= k! [\mathbf{a}_i]_{k+1}. \quad (33b)$$



Thus, from (33) and defining the component

$$[e_i]_{k+1} \triangleq \frac{1}{k!} \lim_{t \rightarrow x_{i-1}^-} g_i^{(k)}(t) \quad (34a)$$

$$= \sum_{j=1}^{d+1} [a_{i-1}]_j (x_{i-1} - x_{i-2})^{j-1-k} \prod_{\ell=1}^k (j - \ell), \quad (34b)$$

we rewrite the equality in (5) as in (6). This is done by dividing both sides of the equality (5) by  $k!$  and renaming the vector component index  $k+1$  as  $q$ .

### C. Proof of Theorem 1

Given a reconstructed function, as in (2), from a sequence  $\mathcal{Z}$ , notice that its  $\text{dom}\{f|_{\mathcal{Z}}\} = \bigcup_{i=0}^{|\mathcal{Z}|} \mathcal{T}_i$  and therefore, its curvature can be equivalently computed as

$$\kappa(f|_{\mathcal{Z}}) = \int_{\bigcup_{i=0}^{|\mathcal{Z}|} \mathcal{T}_i} [f|_{\mathcal{Z}}^{(2)}(t)]^2 dt \quad (35a)$$

$$= \int_{\mathcal{T}_1} [g_1^{(2)}(t)]^2 dt + \dots + \int_{\mathcal{T}_{|\mathcal{Z}|}} [g_{|\mathcal{Z}|}^{(2)}(t)]^2 dt \quad (35b)$$

$$= \sum_{i=1}^{|\mathcal{Z}|} \int_{\mathcal{T}_i} [g_i^{(2)}(t)]^2 dt \quad (35c)$$

$$= \sum_{i=1}^{|\mathcal{Z}|} \kappa(g_i). \quad (35d)$$

### D. Proof of Theorem 2

The curvature of a function section, as in (3), can be computed as

$$\kappa(g_i) = \int_{\mathcal{T}_i} [g_i^{(2)}(t)]^2 dt \quad (36a)$$

$$= \int_{\mathcal{T}_i} [\mathbf{p}_i^{(2)}(t)^\top \mathbf{a}_i]^2 dt \quad (36b)$$

$$= \int_{\mathcal{T}_i} \mathbf{a}_i^\top \mathbf{p}_i^{(2)}(t) \mathbf{p}_i^{(2)}(t)^\top \mathbf{a}_i dt \quad (36c)$$

$$= \mathbf{a}_i^\top \mathbf{M}_i \mathbf{a}_i, \quad (36d)$$

with

$$[\mathbf{M}_i]_{j,k} = \int_{\mathcal{T}_i} [\mathbf{p}_i^{(2)}(t)]_j [\mathbf{p}_i^{(2)}(t)]_k dt. \quad (37)$$

Recall, from (31), that the second derivative with respect to time of the  $j$ th element of the basis function vector (4) is equal to

$$[\mathbf{p}_i^{(2)}(t)]_j = (j-1)(j-2)(t-x_{i-1})^{j-3}. \quad (38)$$

Thereby, it is clear by the relation in (38), that the first two rows and columns of the matrix  $\mathbf{M}$  are zero-valued. Letting  $c = (j-1)(j-2)(k-1)(k-2)$  we can compute the remaining matrix components as

$$[\mathbf{M}_i]_{j,k} = c \int_{x_{i-1}}^{x_i} (t-x_{i-1})^{j-3} (t-x_{i-1})^{k-3} dt \quad (39a)$$

$$= c \int_0^{x_i-x_{i-1}} \tau^{j+k-6} d\tau \quad (39b)$$

$$= c \frac{(x_i-x_{i-1})^{j+k-5}}{j+k-5}. \quad (39c)$$

### E. Derivation of Result 2

The upper incomplete gamma function is defined as

$$\Gamma(s, x) \triangleq \int_x^\infty t^{s-1} \exp(-t) dt. \quad (40)$$

It is worth to mention that when  $s$  is a positive integer then

$$\Gamma(s, x) = (s-1)! \exp(-x) \sum_{k=0}^{s-1} \frac{x^k}{k!}. \quad (41)$$

For the sake of clarity, we omit the dependencies in the notation. We restate the relation in (18) as

$$V_n = \gamma \int_{x_n}^\infty (\boldsymbol{\beta}^\top \mathbf{r}_n(t) - \mu)^2 \exp(-\gamma(t-x_n)) dt \quad (42a)$$

$$= \exp(-\gamma(x_{n-1}-x_n)) \cdot \gamma \int_{x_n}^\infty (\boldsymbol{\beta}^\top \mathbf{r}_n(t) - \mu)^2 \exp(-\gamma(t-x_{n-1})) dt \quad (42b)$$

$$= \exp(\gamma h_n) \gamma \cdot \int_{h_n}^\infty (\boldsymbol{\beta}^\top \hat{\mathbf{r}}_n(\tau) \hat{\mathbf{r}}_n(\tau)^\top \boldsymbol{\beta} - 2\mu \boldsymbol{\beta}^\top \hat{\mathbf{r}}_n(\tau) + \mu^2) \exp(-\gamma\tau) d\tau \quad (42c)$$

$$= \boldsymbol{\beta}^\top \mathbf{R}_n \boldsymbol{\beta} + \boldsymbol{\beta}^\top \mathbf{v}_n + \mu^2. \quad (42d)$$

We arrive to the expression in the step (42b) by adding the zero  $x_{n-1} - x_{n-1}$  within the exponential and rearranging terms. Then in the step (42c), we change the integration variable for  $\tau = t - x_{n-1}$ , denote  $\hat{\mathbf{r}}_n(\tau) = [1, \tau, \dots, \tau^d]^\top$ ,  $h_n = x_n - x_{n-1}$  and expand the terms under the square. Finally, the last step (42d) is obtain by evaluating the integral with

$$[\mathbf{R}_n]_{j,k} = \exp(\gamma h_n) \gamma \int_{h_n}^\infty [\hat{\mathbf{r}}_n(\tau)]_j [\hat{\mathbf{r}}_n(\tau)]_k \exp(-\gamma\tau) d\tau \quad (43a)$$

$$= \exp(\gamma h_n) \gamma \int_{h_n}^\infty \tau^{j+k-2} \exp(-\gamma\tau) d\tau \quad (43b)$$

$$= \exp(\gamma h_n) \gamma^{-j-k+2} \int_{\gamma h_n}^\infty \omega^{j+k-2} \exp(-\omega) d\omega \quad (43c)$$

$$= \exp(\gamma h_n) \frac{\Gamma(j+k-1, \gamma h_n)}{\gamma^{j+k-2}} \quad (43d)$$

$$= \frac{(j+k-2)!}{\gamma^{j+k-2}} \sum_{i=0}^{j+k-2} \frac{(\gamma h_n)^i}{i!}, \quad (43e)$$

where the step (43b) follows after substituting the  $j$ th (or  $k$ th) element of the auxiliary vector valued remainder  $[\hat{\mathbf{r}}_n]_j = \tau^{j-1}$ . Next, we change the integration variable for  $\omega = \gamma\tau$  yielding the step (43c). Lastly, the final step (43e), is obtained by making use of the result in (41).

Similarly, by applying the same steps

$$[\mathbf{v}_n]_j = -2\mu \exp(\gamma h_n) \gamma \int_{h_n}^\infty [\hat{\mathbf{r}}_n(\tau)]_j \exp(-\gamma\tau) d\tau \quad (44a)$$

$$= -2\mu \frac{(j-1)!}{\gamma^{j-1}} \sum_{i=0}^{j-1} \frac{(\gamma h_n)^i}{i!}. \quad (44b)$$

TABLE III

	Myopic	Parametrized	RNN-based
$\mathbf{A}_n$	$\mathbf{M}_n$	$\mathbf{M}_n + \lambda \mathbf{R}_n$	$\mathbf{M}_n + \lambda \mathbf{I}_{d+1}$
$\mathbf{b}_n$	$\mathbf{0}_{d+1}$	$\lambda v_n$	$-2\lambda f_{\theta}(s_n)$

### F. Correctness of Remark 1

The cost function in (22) is convex with respect to the optimization variable  $\beta$  if the matrices  $\mathbf{M}_n$  and  $\mathbf{R}_n$  are positive semidefinite. This is due to, being  $\lambda > 0$ , the sum of such positive definite matrices is positive semidefinite, and therefore the Hessian of the cost w.r.t.  $\beta$ .

Both  $\mathbf{M}_n$  and  $\mathbf{R}_n$  defined in (37) and (43a) respectively, are positive semidefinite thanks to the **Proposition 1** and that  $\gamma$  and  $h_n$  are strictly positive.

### G. Derivation of Result 3

It turns out that all three candidate policies can be evaluated by solving a quadratic convex problem of the form

$$\mathbf{a}_n = \arg \min_{\beta \in \mathbb{R}^{d+1}} \beta^\top \mathbf{A}_n \beta + \mathbf{b}_n^\top \beta \quad (45a)$$

$$\text{subject to: } |\beta^\top \mathbf{p}_n(x_n) - y_n| \leq \epsilon_n, \quad (45b)$$

$$[\beta]_{1:m+1} = \mathbf{e}_n \quad (45c)$$

where  $\mathbf{A}_n \in \mathbf{S}_+^{d+1}$  and  $\mathbf{b}_n \in \mathbb{R}^{d+1}$  take different values depending on the policy. You can see them at Table III.

Notice that we can incorporate the equality constraint (45c) in the objective (45a) by restating

$$\beta = \begin{bmatrix} \mathbf{e}_n \\ \mathbf{0}_{d-m} \end{bmatrix} + \begin{bmatrix} \mathbf{0}_{m+1} \\ \alpha \end{bmatrix}, \quad (46)$$

or equivalently,  $\beta = \mathbf{B}_1 \mathbf{e}_n + \mathbf{B}_2 \alpha$  where  $\mathbf{B}_1 \in \mathbb{R}^{(d+1) \times (m+1)}$  and  $\mathbf{B}_2 \in \mathbb{R}^{(d+1) \times (d-m)}$  are the auxiliary matrices defined in Table I and  $\alpha \in \mathbb{R}^{d-m}$ . In this way, the optimization problem in (45) can be expressed as

$$\mathbf{a}_n = \arg \min_{\alpha \in \mathbb{R}^{d-m}} \alpha^\top \mathbf{B}_2^\top \mathbf{A}_n \mathbf{B}_2 \alpha + (2\mathbf{e}_n^\top \mathbf{B}_1^\top \mathbf{A}_n \mathbf{B}_2 + \mathbf{b}^\top \mathbf{B}_2) \alpha \quad (47a)$$

$$\text{subject to: } |\alpha^\top \mathbf{q}_n - z_n| \leq \epsilon_n, \quad (47b)$$

with  $z_n = y_n - \mathbf{e}_n^\top [\mathbf{p}_n(x_n)]_{1:m+1}$  and  $\mathbf{q}_n = [\mathbf{p}_n(x_n)]_{m+2:d+1}$ .

On the other hand, given an inner product space  $(\mathbb{R}^{d-m}, \langle \cdot, \cdot \rangle_{D_n})$  with  $D_n \in \mathbf{S}_{++}^{d-m}$  and inner product  $\langle \mathbf{u}_1, \mathbf{u}_2 \rangle_{D_n} = \mathbf{u}_1^\top D_n \mathbf{u}_2$ , for any  $\mathbf{u}_1, \mathbf{u}_2 \in \mathbb{R}^{d-m}$  and a vector  $\mathbf{o}_n \in \mathbb{R}^{d-m}$ , it is clear that

$$\|\alpha - \mathbf{o}_n\|_{D_n}^2 = (\alpha - \mathbf{o}_n)^\top D_n (\alpha - \mathbf{o}_n) \quad (48a)$$

$$= \alpha^\top D_n \alpha - 2\mathbf{o}_n^\top D_n \alpha + \mathbf{o}_n^\top D_n \mathbf{o}_n. \quad (48b)$$

Then, by identifying the terms, between the objective in (47a) and (48b), that depend on  $\alpha$  we obtain the relations

$$\mathbf{D}_n = \mathbf{B}_2^\top \mathbf{A}_n \mathbf{B}_2 \quad (49)$$

and

$$\mathbf{o}_n = -(\mathbf{B}_2^\top \mathbf{A}_n \mathbf{B}_2)^{-1} \left( \mathbf{B}_2^\top \mathbf{A}_n \mathbf{B}_1 \mathbf{e}_n + \frac{1}{2} \mathbf{B}_2^\top \mathbf{b}_n \right) \quad (50)$$

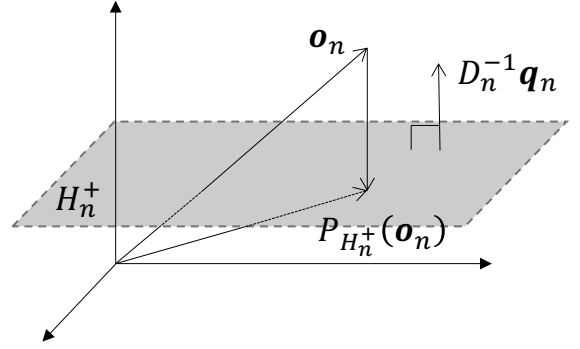


Fig. 7. Conceptualization of a hyperplane projection in the inner product space  $(\mathbb{R}^{d-m}, \langle \cdot, \cdot \rangle_{D_n})$  with  $H_n^+ = \{\mathbf{u} \in \mathbb{R}^{d-m} : \langle \mathbf{u}, D_n^{-1} \mathbf{q}_n \rangle_{D_n} = z_n + \epsilon_n\}$ .

allowing us to equivalently rewrite the optimization problem (47) as in (25).

The  $n$ th (closed) hyperslab, defined as the convex set

$$\mathcal{C}_n \triangleq \{\mathbf{u} \in \mathbb{R}^{d-m} : |\langle \mathbf{u}, D_n^{-1} \mathbf{q}_n \rangle_{D_n} - z_n| \leq \epsilon_n\} \quad (51a)$$

$$= \{\mathbf{u} \in \mathbb{R}^{d-m} : |\mathbf{u}^\top \mathbf{q}_n - z_n| \leq \epsilon_n\}, \quad (51b)$$

can be visualized as the set of all points which belong between and onto the hyperplanes  $H_n^+ = \{\mathbf{u} \in \mathbb{R}^{d-m} : \mathbf{u}^\top \mathbf{q}_n = z_n + \epsilon_n\}$  and  $H_n^- = \{\mathbf{u} \in \mathbb{R}^{d-m} : \mathbf{u}^\top \mathbf{q}_n = z_n - \epsilon_n\}$ .

Based on this observation, the projection onto the  $n$ th hyperslab  $P_{\mathcal{C}_n} : \mathbb{R}^{d-m} \rightarrow \mathbb{R}^{d-m}$  can be computed as

$$P_{\mathcal{C}_n}(\mathbf{u}) = \begin{cases} P_{H_n^+}(\mathbf{u}) & \text{if } \mathbf{u}^\top \mathbf{q}_n > z_n + \epsilon_n \\ \mathbf{u} & \text{if } |\mathbf{u}^\top \mathbf{q}_n - z_n| \leq \epsilon_n \\ P_{H_n^-}(\mathbf{u}) & \text{if } \mathbf{u}^\top \mathbf{q}_n < z_n - \epsilon_n, \end{cases} \quad (52)$$

where  $P_{H_n^+}$  and  $P_{H_n^-}$  denote the projection onto the hyperplanes  $H_n^+$  and  $H_n^-$  (see Fig. 7 as an example) given by

$$P_{H_n^+}(\mathbf{u}) = \mathbf{u} - (\mathbf{u}^\top \mathbf{q}_n - z_n - \epsilon_n) \frac{D_n^{-1} \mathbf{q}_n}{\mathbf{q}_n^\top D_n^{-1} \mathbf{q}_n} \quad (53)$$

and

$$P_{H_n^-}(\mathbf{u}) = \mathbf{u} - (\mathbf{u}^\top \mathbf{q}_n - z_n + \epsilon_n) \frac{D_n^{-1} \mathbf{q}_n}{\mathbf{q}_n^\top D_n^{-1} \mathbf{q}_n} \quad (54)$$

respectively.

Lastly, since the optimization problem (25) corresponds to a hyperslab projection, we can compute its solution by means of (52) as  $\alpha_n = P_{\mathcal{C}_n}(\mathbf{o}_n)$ .

**Remark 2.**  $D_n$  is invertible.

### H. Correctness of Remark 2

From (37) we know that

$$\mathbf{M}_n = \int_{\tau_n} \mathbf{p}_n^{(2)}(t) \mathbf{p}_n^{(2)}(t)^\top dt. \quad (55)$$

Then

$$\mathbf{B}_2^\top \mathbf{M}_n \mathbf{B}_2 = \int_{\tau_n} \mathbf{B}_2^\top \mathbf{p}_n^{(2)}(t) \mathbf{p}_n^{(2)}(t)^\top \mathbf{B}_2 dt. \quad (56)$$

By how  $\mathbf{B}_2 \in \mathbb{R}^{(d+1) \times (d-m)}$  is constructed (see Table I) we know that

$$\mathbf{B}_2^\top \mathbf{p}_n^{(2)}(t) = [\mathbf{p}_n^{(2)}(t)]_{m+2:d+1} \triangleq \mathbf{q}_n^{(2)}(t), \quad (57)$$

with  $\mathbf{p}_n^{(2)}(t) \in \mathbb{R}^{d+1}$  and  $\mathbf{q}_n^{(2)}(t) \in \mathbb{R}^{d-m}$ . Therefore

$$\mathbf{z}^\top \mathbf{B}_2^\top \mathbf{M}_n \mathbf{B}_2 \mathbf{z} = \int_{\tau_n} \mathbf{z}^\top \mathbf{q}_n^{(2)}(t) \mathbf{q}_n^{(2)}(t)^\top \mathbf{z} dt \quad (58a)$$

$$= \int_{\tau_n} (\mathbf{z}^\top \mathbf{q}_n^{(2)}(t))^2 dt > 0, \quad (58b)$$

for any  $\mathbf{z} \in \mathbb{R}^{d-m}$ . Notice that the inequality in (58b) holds because the components of  $\mathbf{q}_n^{(2)}(t)$  are linearly independent (polynomial of different degree), see **Proposition 1**. For clarity, recall that from (38) and (57) we can explicitly write each component of  $\mathbf{q}_n^{(2)}(t)$  as

$$[\mathbf{q}_n^{(2)}(t)]_j = (j+m+1)(j+m)(t-x_{n-1})^{j+m-1}. \quad (59)$$

Lastly, regardless the chosen policy, the matrix  $\mathbf{D}_n$  consists of a sum of a positive definite and a positive (semi)-definite matrix, therefore  $\mathbf{D}_n$  is positive definite and invertible.

## REFERENCES

- [1] J. Gama, *Knowledge discovery from data streams*. CRC Press, 2010.
- [2] U. Sivarajah, M. M. Kamal, Z. Irani, and V. Weerakkody, "Critical analysis of big data challenges and analytical methods," *Journal of Business Research*, vol. 70, pp. 263–286, 2017.
- [3] J. Gama, "A survey on learning from data streams: current and future trends," *Progress in Artificial Intelligence*, vol. 1, no. 1, pp. 45–55, 2012.
- [4] A. A. Benczur, L. Kocsis, and R. Pálovics, "Online machine learning in big data streams," *arXiv preprint arXiv:1802.05872*, 2018.
- [5] M. Mohammadpoor and F. Torabi, "Big data analytics in oil and gas industry: An emerging trend," *Petroleum*, vol. 6, no. 4, pp. 321–328, 2020.
- [6] M. reza Akhondi, A. Talevski, S. Carlsen, and S. Petersen, "Applications of wireless sensor networks in the oil, gas and resources industries," in *2010 24th IEEE International Conference on Advanced Information Networking and Applications*, pp. 941–948, IEEE, 2010.
- [7] O. Soft, "Pi system," URL: <https://www.osisoft.com/pi-system>, 1980.
- [8] M. Cui, J. Zhang, A. R. Florita, B.-M. Hodge, D. Ke, and Y. Sun, "An optimized swinging door algorithm for identifying wind ramping events," *IEEE Transactions on Sustainable Energy*, vol. 7, no. 1, pp. 150–162, 2015.
- [9] F. Xiaodong, C. Changling, L. Changling, and S. Huihe, "An improved process data compression algorithm," in *Proceedings of the 4th World Congress on Intelligent Control and Automation (Cat. No. 02EX527)*, vol. 3, pp. 2190–2193, IEEE, 2002.
- [10] M. A. Khan, J. W. Pierre, J. I. Wold, D. J. Trudnowski, and M. K. Donnelly, "Impacts of swinging door lossy compression of synchrophasor data," *International Journal of Electrical Power & Energy Systems*, vol. 123, p. 106182, 2020.
- [11] E. Meijering, "A chronology of interpolation: from ancient astronomy to modern signal and image processing," *Proceedings of the IEEE*, vol. 90, no. 3, pp. 319–342, 2002.
- [12] E. Waring, "VII. problems concerning interpolations," *Philosophical transactions of the royal society of London*, no. 69, pp. 59–67, 1779.
- [13] O. Guven, A. Eftekhar, W. Kindt, and T. G. Constantinou, "Computationally efficient real-time interpolation algorithm for non-uniformly sampled biosignals," *Healthcare technology letters*, vol. 3, no. 2, pp. 105–110, 2016.
- [14] S. A. Bazaz and B. Tondur, "Minimum time on-line joint trajectory generator based on low order spline method for industrial manipulators," *Robotics and Autonomous Systems*, vol. 29, no. 4, pp. 257–268, 1999.
- [15] T. Kröger, *On-Line Trajectory Generation in Robotic Systems: Basic Concepts for Instantaneous Reactions to Unforeseen (Sensor) Events*, vol. 58. Springer, 2010.
- [16] I. J. Schoenberg, "Contributions to the problem of approximation of equidistant data by analytic functions," in *IJ Schoenberg Selected Papers*, pp. 3–57, Springer, 1988.
- [17] L. Schumaker, *Spline functions: basic theory*. Cambridge University Press, 2007.
- [18] J. M. de Carvalho and J. V. Hanson, "Real-time interpolation with cubic splines and polyphase networks," *Canadian Electrical Engineering Journal*, vol. 11, no. 2, pp. 64–72, 1986.
- [19] R. Debski, "Real-time interpolation of streaming data," *Computer Science*, vol. 21, no. 4, 2020.
- [20] G. Wahba, *Spline models for observational data*. SIAM, 1990.
- [21] A. J. Smola and B. Schölkopf, *Learning with kernels*, vol. 4. Citeseer, 1998.
- [22] A. Nosedal-Sanchez, C. B. Storlie, T. C. Lee, and R. Christensen, "Reproducing kernel hilbert spaces for penalized regression: A tutorial," *The American Statistician*, vol. 66, no. 1, pp. 50–60, 2012.
- [23] J. Kivinen, A. J. Smola, and R. C. Williamson, "Online learning with kernels," *IEEE transactions on signal processing*, vol. 52, no. 8, pp. 2165–2176, 2004.
- [24] S. Van Vaerenbergh, J. Via, and I. Santamaría, "A sliding-window kernel rls algorithm and its application to nonlinear channel identification," in *2006 IEEE International Conference on Acoustics Speech and Signal Processing Proceedings*, vol. 5, pp. V–V, IEEE, 2006.
- [25] K. Slavakis, P. Bouboulis, and S. Theodoridis, "Online learning in reproducing kernel hilbert spaces," in *Academic Press Library in Signal Processing*, vol. 1, pp. 883–987, Elsevier, 2014.
- [26] E. Ruiz-Moreno and B. Beferull-Lozano, "Tracking of quantized signals based on online kernel regression," in *2021 IEEE 31st International Workshop on Machine Learning for Signal Processing (MLSP)*, pp. 1–6, IEEE, 2021.
- [27] G. Kimeldorf and G. Wahba, "Some results on tchebycheffian spline functions," *Journal of mathematical analysis and applications*, vol. 33, no. 1, pp. 82–95, 1971.
- [28] Z. Wang, K. Crammer, and S. Vucetic, "Breaking the curse of kernelization: Budgeted stochastic gradient descent for large-scale svm training," *The Journal of Machine Learning Research*, vol. 13, no. 1, pp. 3103–3131, 2012.
- [29] A. Singh, N. Ahuja, and P. Moulin, "Online learning with kernels: Overcoming the growing sum problem," in *2012 IEEE International Workshop on Machine Learning for Signal Processing*, pp. 1–6, IEEE, 2012.
- [30] A. Koppel, A. S. Bedi, K. Rajawat, and B. M. Sadler, "Optimally compressed nonparametric online learning: Tradeoffs between memory and consistency," *IEEE Signal Processing Magazine*, vol. 37, no. 3, pp. 61–70, 2020.
- [31] S. N. Shukla and B. M. Marlin, "Interpolation-prediction networks for irregularly sampled time series," *arXiv preprint arXiv:1909.07782*, 2019.
- [32] Z. Che, S. Purushotham, K. Cho, D. Sontag, and Y. Liu, "Recurrent neural networks for multivariate time series with missing values," *Scientific reports*, vol. 8, no. 1, pp. 1–12, 2018.
- [33] K. Cho, B. Van Merriënboer, C. Gulcehre, D. Bahdanau, F. Bougares, H. Schwenk, and Y. Bengio, "Learning phrase representations using rnn encoder-decoder for statistical machine translation," *arXiv preprint arXiv:1406.1078*, 2014.
- [34] I. Jovanovic and B. Beferull-Lozano, "Oversampled a/d conversion and error-rate dependence of nonbandlimited signals with finite rate of innovation," *IEEE Transactions on Signal Processing*, vol. 54, no. 6, pp. 2140–2154, 2006.
- [35] S. N. Wood, *Generalized additive models: an introduction with R*. CRC press, 2017.
- [36] A. Agrawal, B. Amos, S. Barratt, S. Boyd, S. Diamond, and Z. Kolter, "Differentiable convex optimization layers," *arXiv preprint arXiv:1910.12430*, 2019.
- [37] S. Boyd, S. P. Boyd, and L. Vandenberghe, *Convex optimization*. Cambridge university press, 2004.
- [38] D. Bertsekas, *Reinforcement learning and optimal control*. Athena Scientific, 2019.
- [39] L. Medsker and L. C. Jain, *Recurrent neural networks: design and applications*. CRC press, 1999.
- [40] S. Hochreiter and J. Schmidhuber, "Long short-term memory," *Neural computation*, vol. 9, no. 8, pp. 1735–1780, 1997.
- [41] E.-G. Talbi, "A taxonomy of metaheuristics for bi-level optimization," in *Metaheuristics for bi-level optimization*, pp. 1–39, Springer, 2013.
- [42] P. J. Werbos, "Backpropagation through time: what it does and how to do it," *Proceedings of the IEEE*, vol. 78, no. 10, pp. 1550–1560, 1990.
- [43] I. Goodfellow, Y. Bengio, and A. Courville, *Deep learning*. MIT press, 2016.
- [44] C. Florescu and C. Igel, "Resilient backpropagation (rprop) for batch-learning in tensorflow," <https://openreview.net/forum?id=r1R0o7yDz>, 2018.

- [45] A. Brand, L. Allen, M. Altman, M. Hlava, and J. Scott, "Beyond authorship: attribution, contribution, collaboration, and credit," *Learned Publishing*, vol. 28, no. 2, pp. 151–155, 2015.